Research article

Atomic-scale and optical investigation of nanostructured Er disilicates in silica

S. Guehairia [a], R. Demoulin [a], H. Merabet [b], P. Pareige [a], J. Cardin [c], C. Labbé [c], M. Carrada [d], F. Gourbilleau [c], E. Talbot [a],*

[a] *Normandie Univ, UNIROUEN, INSA Rouen, CNRS, Groupe de Physique des Matériaux, 76000 Rouen, France*
[b] *Physics Program, Department of Mathematics, Statistics and Physics, College of Arts and Sciences, Qatar University, P.O. box 2713, Doha, Qatar*
[c] *CIMAP, CNRS, ENSICAEN, UNICAEN, CEA, Normandie Univ, 14000 Caen, France*
[d] *CEMES-CNRS, Université de Toulouse, 29 rue Jeanne Marvig, BP 94347, F-31055 Toulouse, France*

ARTICLE INFO

ABSTRACT

The optical and structural properties of Er-doped Silicon oxide based thin films elaborated by RF magnetron sputtering were investigated as a function of annealing treatment. Atom Probe Tomography and Transmission electron microscopy were used to analyze the position of rare-earth ions as well as the phase separation occurring in the layer in order to provide a complete picture of the nanostructure. The emission properties of Er^{3+} ions were investigated using cathodoluminescence (CL) spectroscopy. The high doping level of Er ions in silicon oxide matrix leads to a phase decomposition of pure SiO_2 and $Er_2Si_2O_7$ phases with a nanostructure which is influenced by the annealing treatment. It results on different emission intensities in ultraviolet or infrared ranges. The relationship between the nanostructuration observed and the optical properties is discussed in regards of annealing treatment.

1. Introduction

Rare earth doping of oxides is of particular interest for the development of new technologies in the fields of optoelectronics and photonics [1–4]. In particular, the case of erbium doping of silicon oxide is a material of choice due to its effective luminescence at the 1.54 μm wavelength used for optical communication fibers [5–8]. In addition, the excitation of Er-doped insulating materials cannot be effective due to the small effective cross section for resonant excitation [9]. In recent years, the main approach to improve the efficiency of Er luminescence and avoid the need for high excitation powers has been to take advantage of energy transfer from silicon nanocrystals [8,10–13]. However, it has been shown that only ions in close proximity to Si-ncs can be excited and that the optically active concentration of rare earth ions remains very low [14].

Moreover, the solubility limit of erbium in the silica-based matrix as well as the processing and thermal annealing parameters strongly limit the increase of Er concentrations and enhancements of luminescence. Indeed, high Erbium doping leads to the formation of precipitates which are responsible for signal extinction [15–17]. It

has been recently demonstrated that in 1–2 at. % Er doped silicon rich silicon oxide, the annealing treatment leads to the formation of Si-ncs but also to the formation of Er-rich particles which are responsible for the luminescence quenching. However, structural and chemical analyses at the atomic scale have shown that under certain conditions, these particles correspond to Er silicate phases of nanometric dimensions. This last phase is known to be optically active and allows to reach high Erbium concentrations (10^{22} at./cm^3). In particular, Erbium disilicates $Er_2Si_2O_7$ can exhibit an intense luminescence which depends of the polymorph [18,19]. Moreover, it was recently demonstrated that pyrosilicate C-$Er_2Si_2O_7$ can present near-infrared up-conversion emission [20]. But to control the optical properties of these phases, it is also necessary to control finely their crystallization and avoid the presence of defects that can quench the luminescence [21–23].

In this paper, we propose to study the diffusion of Er ions in silica matrices containing very high concentrations of erbium in order to control the formation of nanometric Er silicate phases. Phase evolution was studied by microscopy at the atomic level and correlated with the optical properties.

---

* Corresponding author.
E-mail address: etienne.talbot@univ-rouen.fr (E. Talbot).

2. Experimental

Er-rich doped SiO_2 containing ~10 at. % of Er were deposited on (100)-oriented and double side polished 2- Si wafer by RF magnetron co-sputtering of pure 2- SiO_2 and Er_2O_3 targets in a pure Ar plasma. The power densities applied on the targets were 4.4 and 2.8 $W.cm^{-2}$, respectively, while the substrate has been maintained at 500℃ during the deposition run. The refractive index at 1.95 eV has been determined from ellipsometery measurements by fitting the measured ψ and Δ ellipsometric angles as a function of the energy using DeltaPsi software provided by Horiba company. The refractive index of the film after deposition is found to be 1.61 at 632 nm. The value higher than that of SiO_2 (1.45) attests of the incorporation of Er atoms in the host matrix. The wafers were cut in three pieces, with one kept as as-deposited film (AD) whereas the two others were submitted to an annealing treatment at a temperature of 1000℃ during 4 h by classic treatment annealing (CTA) or 1200℃ during 30 s by rapid annealing treatment (RTA), both under pure N_2 atmosphere. Atom Probe Tomography (APT) experiments were performed using a laser-assisted wide-angle tomographic atom probe (LAWATAP - CAMECA) including femtosecond laser pulses in UV range (343 nm, 350 fs) and a 0.62 detector yield. For these analyses, samples were previously prepared using Plasma-FIB - Helios (FEI) by the lift out and annular milling process in order to have a radius curve smaller than 50 nm [24]. The APT data were treated with the software GPM3dSoft.

TEM observations were performed on cross-sectional (CS) specimen using a field emission FEI TecnaiTM F20 microscope operating at 200 kV, equipped with a spherical aberration corrector.

The photoluminescence (PL) spectra in the Vis-NIR region were obtained using an 280 nm excitation wavelength that is non-resonant with Er^{3+} ions.

The cathodoluminescence (CL) measurements were performed on a HORIBA HCLUE system in situ of a JEOL 7900 F scanning electron microscope (SEM). The optical emissions were collected in ultraviolet-visible (UV–vis, 300–1000 nm) and infrared (IR, 1100–1750 nm) ranges using 600 and 150-grooves grating, respectively. The high voltage was 10 kV and the probe current was 20 nA. The spectral resolution is lower than 0.7 nm.

3. Results and discussion

3.1. Optical properties

The PL spectra acquired on as-deposited and annealed samples in the Vis-NIR region (500–1200 nm) are reported on Fig. 1. The highest PL intensity is detected for the sample annealed by rapid thermal annealing approach at 1200℃ for which two broad luminescence bands are detected. The first one is centered at around 710 nm and has a full width at half maximum (FWHM) of 150 nm whereas the second is centered at around 950 nm with a FWHM of 155 nm. These two luminescence bands can be attributed to intra-4*f* transitions of Er^{3+} ions and will be discussed later. The PL emission drops by a factor 8 between RTA and CTA samples and by decreasing annealing temperature. In the as-deposited state, no luminescence is detected.

CL emission has been studied taking advantage that electron excitation is broadband compared to photons, which leads to different recombination pathways and corresponding spectral signature. In addition, the high energy deposited by the electron beam generally favors a better luminescence yield. Fig. 2 shows the cathodoluminescence spectra of Er doped silicon oxide in the UV–vis region (300–1000 nm) for the three distinct samples at room temperature (300 K).

To compare the intensities, all of the spectra were acquired under the same conditions. In all the case, the recorded optical emission exhibits several groups of well-resolved luminescence peaks
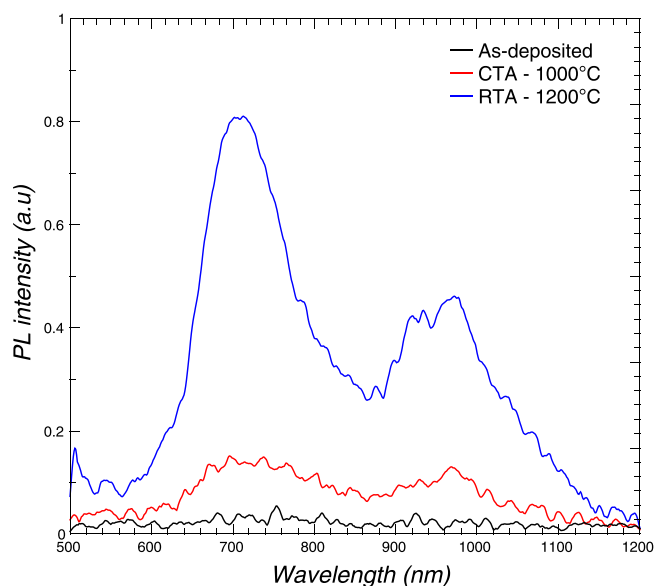

Fig. 1. PL spectra in Visible-NIR range of Er^{3+}-doped SiO_2 thin films as deposited, CTA and RTA samples in the range 500–1200 nm.

associated to intra-4*f* transitions of Er^{3+} ions. The wavelength and the associated intra-4*f* transitions are reported in Table 1. Most of the CL peaks involve transitions to the $^4I_{15/2}$ ground state.

The as-deposited sample showed six large CL peaks attributed to the transitions in Er^{3+} ions. The most intense correspond to the doublet located at 547–557 nm which can be attributed to the transition $^2H_{11/2} \rightarrow ^4I_{15/2}$. This peak is the most intense in all our samples (Fig. 2.a). The other bands are located at 382, 408, 523, 659, 701 and 850 nm and correspond to the transitions $^4G_{11/2} \rightarrow ^4I_{15/2}$, $^2H_{9/2} \rightarrow ^4I_{15/2}$, $^2H_{11/2} \rightarrow ^4I_{15/2}$, $^4F_{9/2} \rightarrow ^4I_{15/2}$, $^2H_{9/2} \rightarrow ^4I_{11/2}$ and $^4S_{3/2} \rightarrow ^4I_{13/2}$, respectively. It should be noted that all the transition corresponds to a de-excitation to the ground state except for the emission at 701 and 850 nm.

The CL spectrum of the sample annealed with a classical method (CTA) is similar to that of the as-deposited sample. With annealing, however, the CL intensity of all the peaks increases by a factor of about 1.4–1.5. This increase can be attributed to a reorganization of the host matrix with temperature which results in the recovery of the non-radiative defects that are present in the non-annealed sample. This atomic rearrangement has also favored the appearance of an additional broad line that is detected at 980 nm, associated to the $^4I_{11/2} \rightarrow ^4I_{15/2}$ transition. After an annealing at 1200℃, the emission spectrum exhibits more sharp peaks than for the two others samples which can be related to a different environment of Er^{3+} emission centers in the films (Fig. 2.b, c and d). Moreover, it can be noted that emission peaks previously detected at 382 and 408 nm have disappeared after such a high annealing treatment. An additional luminescence signature is detected in the band 753–769 nm region corresponding's to the transition $^2P_{3/2} \rightarrow ^4S_{3/2}$ transition. To observe more precisely the splitting of CL line emission with the RTA process, spectra of CTA and RTA samples on selected wavelength ranges are presented on Fig. 2.b, c and d. The sharpening of CL peaks after RTA annealing is clearly visible. Such a feature could be the result of the modification of Er^{3+} ions environment, specifically a crystallization of the matrix and/or of the phase containing Er atoms. A significant decrease of the intensity of the luminescence peak at 523 nm is also observed (Fig. 2.b). Simultaneously, a rise in the 980 nm emission is seen (Fig. 2.d).

CL spectra show more numerous and more resolved emission lines related to the difference of recombination mechanism between PL and CL. The photon excitation can only probe a broad band
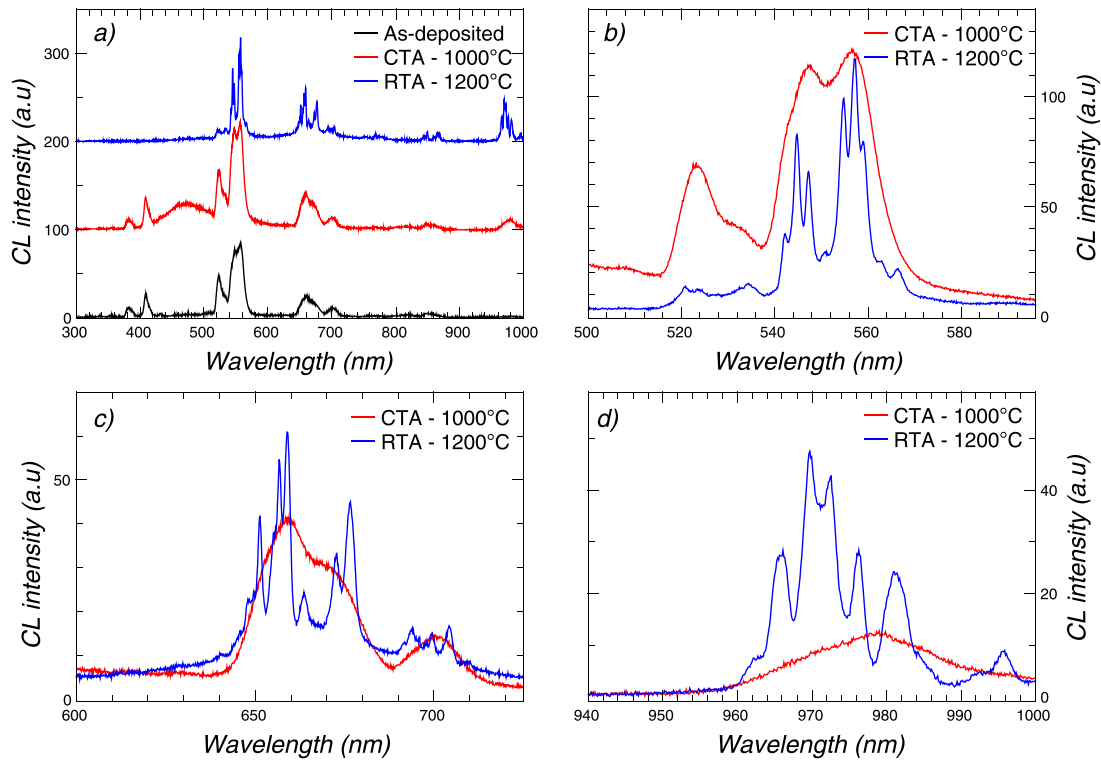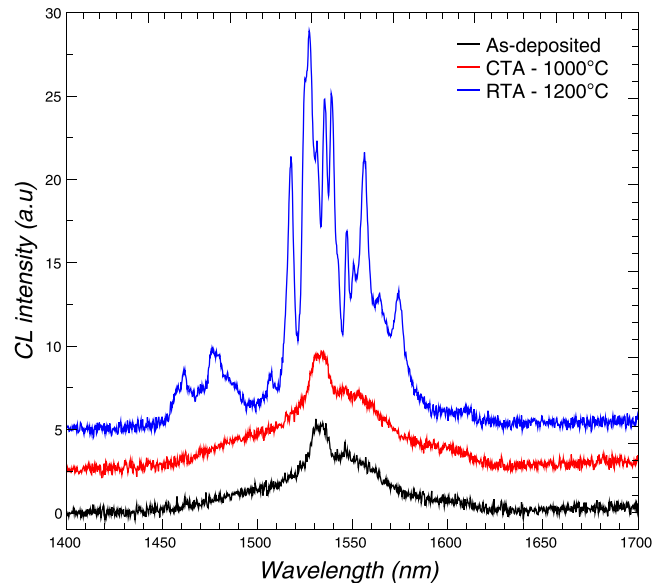
Fig. 2. CL spectra in UV–vis range of Er^{3+}-doped SiO_2 thin films: a) as deposited, CTA and RTA samples in the range 300–1000 nm. b), c) and d) correspond to selected wavelength ranges for CTA and RTA samples.

Table 1
Electronic transitions observed in CL for Erbium ions in the three samples.

| Transition	Wavelength (nm)		
	As-deposited	CTA	RTA
$^4G_{11/2} \rightarrow {}^4I_{15/2}$	382	382	N.V
$^2H_{9/2} \rightarrow {}^4I_{15/2}$	408	408	N.V.
$^4F_{3/2-5/2} \rightarrow {}^4I_{15/2}$	432	432	N.V
$^2H_{11/2} \rightarrow {}^4I_{15/2}$	523	523	525–535
$^4S_{3/2} \rightarrow {}^4I_{15/2}$	547–557	547–579	544–565
$^4F_{9/2} \rightarrow {}^4I_{15/2}$	659–670	659–670	651–660–676
$^2H_{9/2} \rightarrow {}^4I_{11/2}$	701	701	694–702
$^2P_{3/2} \rightarrow {}^4S_{3/2}$	N.V.	N.V.	753–769
$^4I_{9/2} \rightarrow {}^4I_{15/2}$	815	815	N.V.
$^4S_{3/2} \rightarrow {}^4I_{13/2}$	849–860	849–860	843–869
$^4I_{11/2} \rightarrow {}^4I_{15/2}$	N.V.	980	966–996
$^4I_{13/2} \rightarrow {}^4I_{15/2}$	1533–1547	1533–1547	1460–1575

including $^4F_{9/2} \rightarrow {}^4I_{15/2}$ and $^4H_{9/2} \rightarrow {}^4I_{11/2}$ and a band related to the $^4I_{11/2} \rightarrow {}^4I_{15/2}$ transition.

CL spectra recorded in the infra-red range for the 3 samples are presented on Fig. 3. As previously observed in the UV–vis range, the as-deposited and CTA samples exhibit a similar optical response in CL experiment. An IR-luminescence emission located at 1533 nm with a shoulder at 1550 nm is recorded with a more intense response after a CTA annealing treatment. Theses peaks can be attributed to the $^4I_{13/2} \rightarrow {}^4I_{15/2}$ transition. According to the behavior observed in the UV–VIS range, we observed more resolved peaks in the region 1460–1575 nm for the layer annealed by means of RTA setup, as well as an increase of the emission intensity around 1.55 μm. The differences observed on the CL spectra between the two annealed samples, in particular the evolution from broad peak to narrow ones in the emission spectra, can be due to a crystallization of the sample leading to a change on the Er^{3+} atoms environments on the RTA sample.

Fig. 3. CL spectra in IR range of Er^{3+}-doped SiO_2 thin films in as deposited, CTA and RTA-samples.

Thus, AD and CTA samples have a classical luminescence spectral signature of Er in a SiO_2 matrix with or without Si-ncs [25] or silicates [26]. In terms of spectral signature, it is not possible for these samples to formulate hypotheses on the amorphous or crystallized nature of the sample, and/or the presence of secondary phases like erbium silicates [27]. On the contrary, the spectral response of the RTA sample, i.e. the splitting of the peaks and in particular the transition in the infra-red allows us to suggests the presence of a crystalline phase of Erbium pyrosilicate. Y. Gao *et al.* have recently
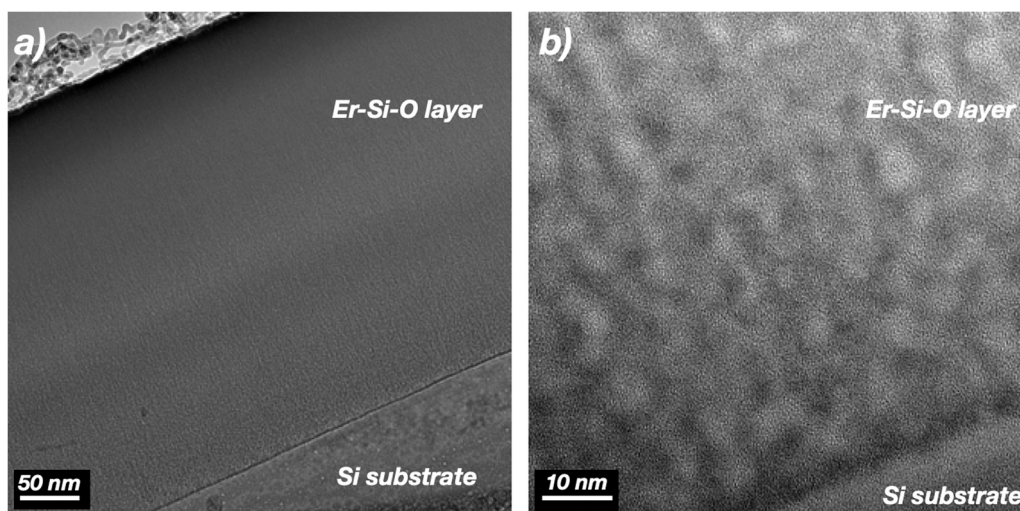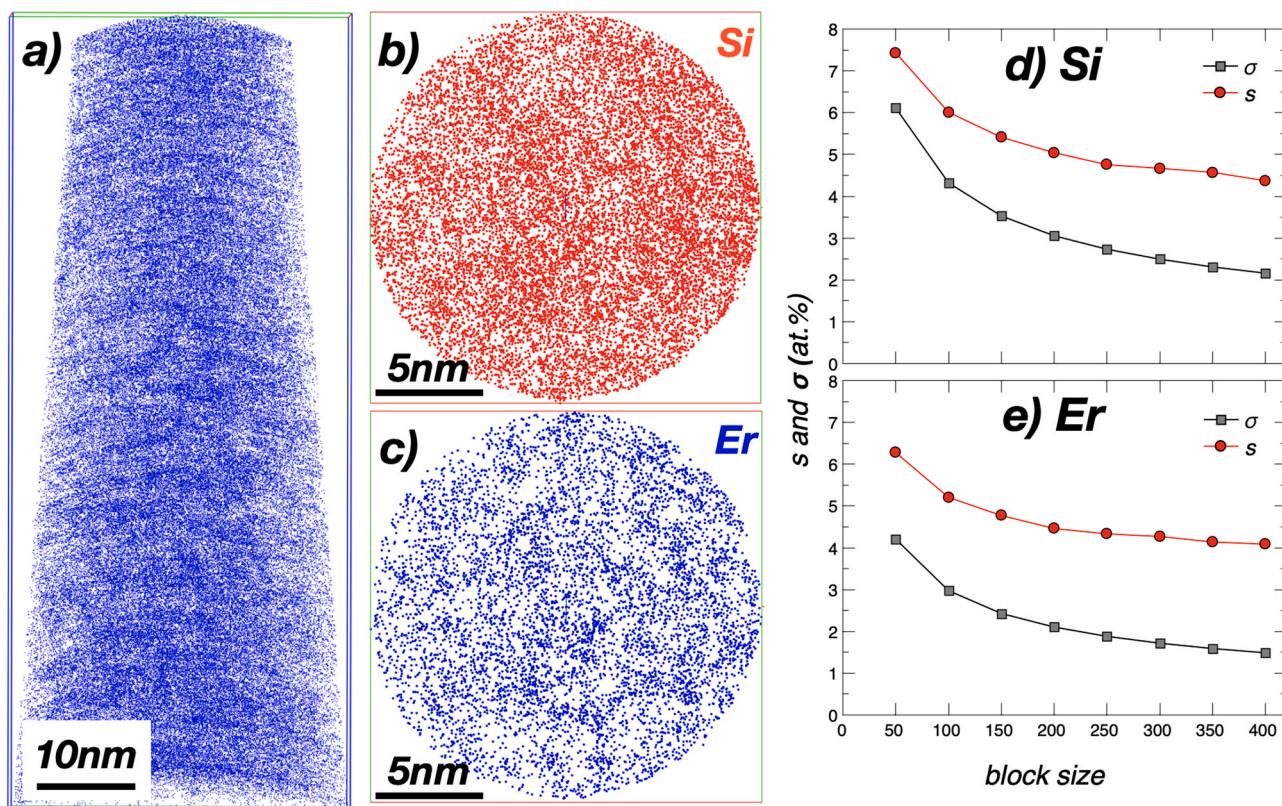
Fig. 4. Cross-section TEM images of the as-deposited Er-rich SiO$_2$ layers (a) at low magnification (Bright Field imaging) and (b) in High Resolution mode.

evidenced the influence of the polymorphic form of Er$_2$Si$_2$O$_7$ silicates phases in the IR range allowing a spectral identification of polymorph in Erbium doped silicon oxide [23,28]. Based on the IR-CL spectrum, we can expect the presence of the monoclinic phase *y*-Er$_2$Si$_2$O$_7$, or α-Er$_2$Si$_2$O$_7$ or mixture of both [26,29]. These findings can be explained by the influence of the crystal field surrounding Er^{3+} ions related to the evolution of the structure under annealing treatment. It is widely known that erbium doping of silica or silicon rich silica can result in: i) dopant precipitation [30] ii) silicon nanocrystals formation [8] iii) Er silicates phases formation [16], depending on the fabrication conditions and annealing process.

3.2. Composition and structures at atomic scale

Chemical and structural characteristics of the three samples (as deposited, annealed by classical or rapid treatment) have been investigated by Transmission Electronic Microscopy and Atom Probe Tomography. Fig. 4 presents cross-section TEM images of the sample in the as-deposited state. At low magnification (Bright Field imaging), the sample appears to be inhomogeneous and elongated bright contrast structures can be observed along the growth direction (Fig. 4.a) No interfacial layer is detected at the interface with the Si substrate. At higher magnification (High Resolution imaging),

Fig. 5. a) 3D mapping of Er atoms, b, c) cross-sectional views extracted from 3D volume, d and e: statistical tests of randomness of Si atoms (d) and Er atoms (e) in the as-deposited sample.
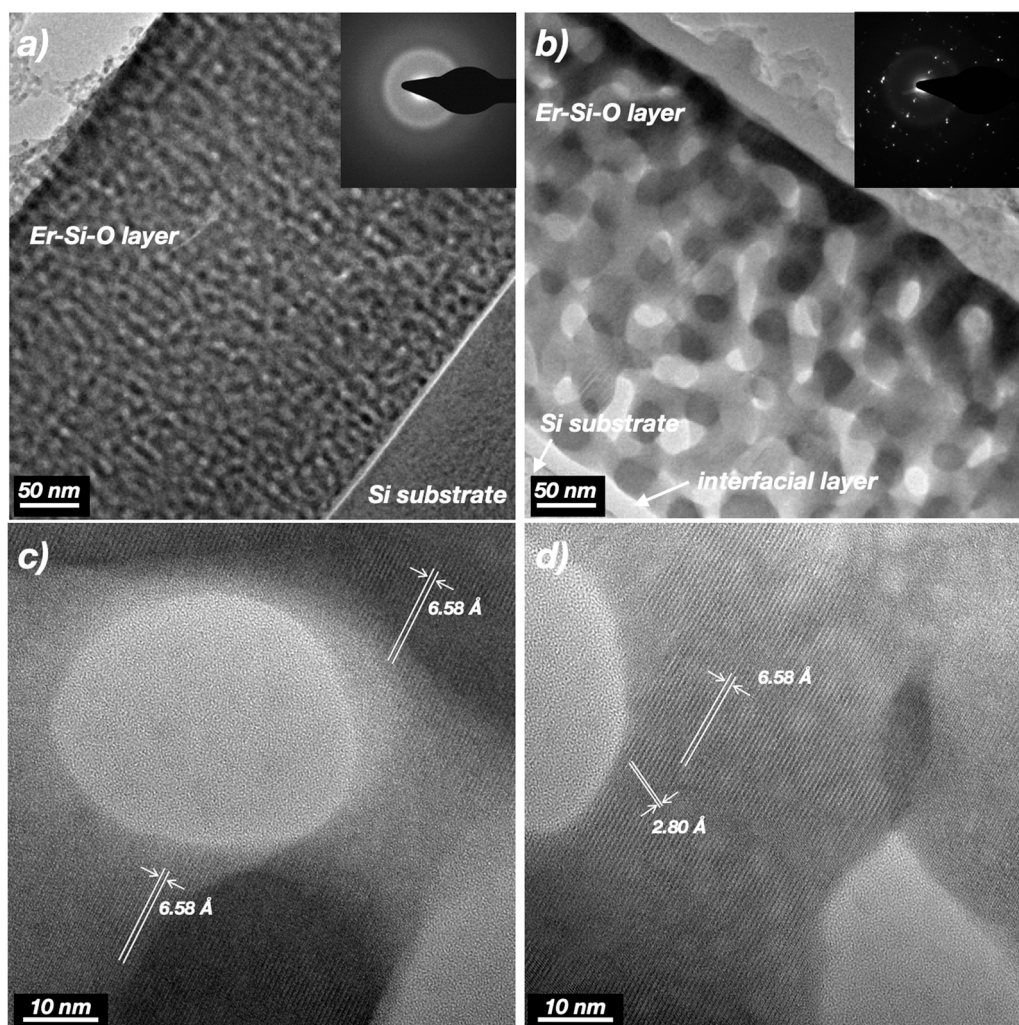
Fig. 6. Cross-section TEM images and diffraction patterns (inset) of the Er-rich SiO$_2$ layers after CTA (a) or RTA (b, c and d) annealing.

Fig. 4.b reveals bright and dark contrasts zones that are the signature of inhomogeneities at the nanometer scale. The darkest contrast corresponds to Er richer zones. Note that TEM experiments on the as-deposited sample have evidenced an amorphous nature of the grown layer (not shown here). This characteristic may be the reason for the broad CL emission observed (Figs. 2 and 3) and therefore in coherence with the fact that the signal of the AD sample is the lowest of the three ones.

Fig. 5 shows the result from APT analysis of the AD sample. The 3D mapping of the Er in the analyzed volume (Fig. 5.a) and cross-sectional views extracted from 3D reconstructed volume (Fig. 5.b and c) yield similar results to TEM analysis. We used the Thuvander approach [31] to perform statistical tests on randomness based on the mapping of each species in the analyzed volume, and the results for Si and Er atoms are shown in Fig. 5.d and e, respectively. The main objective of this test is to compare the standard error (s) of the frequency distribution of an element (Si or Er in this case) computed from 3D volume obtained by APT and the standard deviation (sigma) of the binomial distribution (random case). The results of the test (Fig. 5.d and e) evidenced a non-random distribution of Si and Er atoms which can explain the inhomogeneity observed in TEM micrographs (Fig. 5). This reveals a preferential affinity between Er and Si atoms from the deposit in the case of high Er concentration. This phenomenon has already been observed before and can be explain by the introduction dopant cell which is at 600 °C, favoring the migration and aggregation of Er atoms [16,17]. In addition, the mean

chemical composition of the analyzed sample was computed from APT analysis. The measured concentrations are: $X_{Si} = 21.8 \pm 1.0$ at. %; $X_O = 68.9 \pm 1.0$ at. % and $X_{Er} = 9.3 \pm 1.0$ at. %. We can note that the overall composition of the sample analyzed by APT does not vary between AD-, CTA- or RTA-samples.

Fig. 6 presents cross-section TEM images of the samples that have been annealed using either classical or rapid methods. Following an annealing treatment at 1000°C (CTA) or 1200°C (RTA), the two annealed samples are obviously inhomogeneous. Both presents an interfacial layer at the interface with the Si substrate. The presence of bright and dark contrast in the layers is due to phase separation into Er poor (bright) and Er rich (dark) zones. The phase separation results in the presence of two sublattices in both the CTA sample (Fig. 6.a) and the RTA sample (Fig. 6.b), but the bright and dark observed zones have larger dimensions in the last case. In addition, the amorphous and crystalline natures of the CTA- and RTA-samples are demonstrated by the selected area electron diffraction patterns displayed in the inset of Fig. 6. A closer observation by HR-TEM of the RTA sample (Fig. 6.c and d) evidenced the presence of an amorphous Er-poor phases (bright contrast) and crystallized Er-rich phases (dark contrast). These TEM observations confirm the structural evolution suspected to be at the origin of the results obtained in CL.

The diffraction pattern shown in the inset of Fig. 6 can be indexed with respect to the triclinic (B-type $P\bar{1}$) polymorph erbium disilicate Er$_2$Si$_2$O$_7$ phase. A detailed description of the polymorphs for rare-
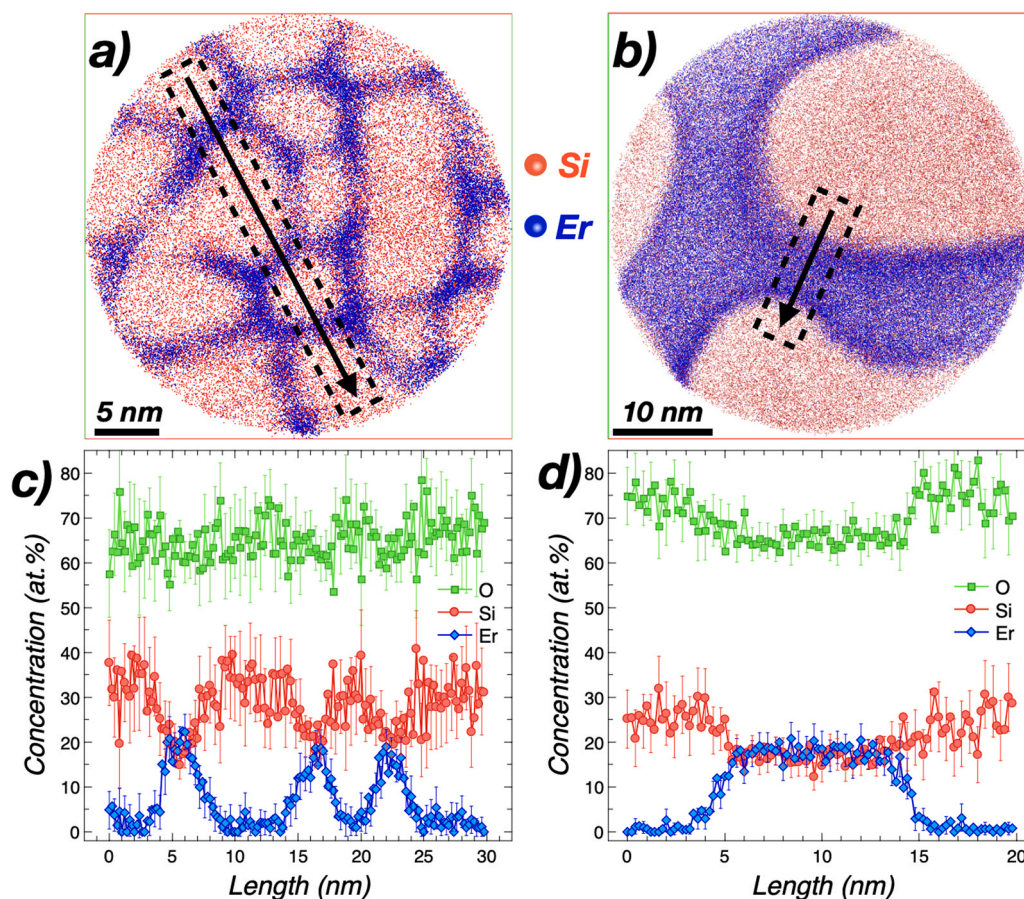
Fig. 7. Three dimensional mapping cross section of CTA (a) and RTA (b) samples and composition accross silicon and erbium rich zones (c,d).

earth disilicate compound can be found in the paper of Felsche [32]. The triclinic structure is caracterized by lattice constants: $a = 6.583$ Å, $b = 6.609$ Å, $c = 12.000$ Å, $\alpha = 94.50°$, $\beta = 90.57°$ and $\gamma = 91.79°$ [32,33]. The associated (100) and (002) planes of the B-type $Er_2Si_2O_7$ are visible on Fig. 6.c and d. Our finding are in agreement with those of Kepinski *et al.* who have previously evidenced by XRD and TEM the formation of B-$Er_2Si_2O_7$ in Er_2O_3:SiO_2 systems annealed at 1000°C or higher [34]. Gao et al. have also observed that the triclinic phase is the most stable one for annealing temperatures above 1100°C. Traces of Er_2SiO_5 phases have never been observed although this phase is often observed when growing on silica or silicon [35]. Also, no other polymorph were identified in the TEM analysis.

In order to get a better understanding of the evolution of the nanostructure of the samples after annealing, it is necessary to perform 3D mapping and composition measurements. Fig. 7.a and b present cross sections mapping of CTA and RTA samples obtained by APT analyses. We note a segregation and the presence of two phases, one Er poor and one Er rich whose structure is thinner in the CTA sample and wider in the RTA one in agreement with TEM observations. Compositions profiles, presented in Fig. 7.c and d, were computed across the two zones in order to determine the chemistry of the Er poor and rich zones as well as its characteristic dimensions. Whatever the annealing process, the Er-rich phase corresponds to the Erbium silicate $Er_2Si_2O_7$, with a width of 2–4 nm in the case of CTA reaching 15–20 nm after a RTA process. The Er-poor zones can be attributed unambiguously to the SiO_2 phase.

3.3. Discussion

Plentiful studies on Er doped silicon oxide have already shown that the optical properties of Er^{3+} ions are directly governed by the

structural evolution depending on dopant concentration, composition of silicon oxide and/or annealing strategies. For the case of high Er concentration, i.e. greater than the solubility of Er in silica, all of them agree that rare-earth atoms segregate to form Er-oxide [36] or Er-silicates particles [16]. Here, the nanostructures and its evolutions under annealing treatment observed in this work by transmission electron microscope and atom probe tomography help us to understand the optical properties obtained by photo- and cathodoluminescence spectroscopy (Figs. 2 and 3). Whatever the type of annealing treatment, rapid or classical, the Er ions diffused until the formation of the stable silicate $Er_2Si_2O_7$ interconnected to a silica one. Both the 3D atomic mapping obtained by APT and the TEM images confirm the presence of these two phases in the two annealed samples. Furthermore, the conventionally annealed sample has a coalescence leading to a honeycomb-like structure of the erbium-rich phase while the fast annealed one at higher temperature has a higher coalescence leading to a larger erbium-rich phase. We found that CTA and RTA samples show a similar luminescence intensity in CL indicating that even the structure remains amorphous in classical annealing treatment, Er ions are mainly optically active in $Er_2Si_2O_7$ amorphous phase. For RTA process, the Er-related cathodoluminescence presents multiple peaks for each transition lines due to the Stark splitting of the energy levels of Er^{3+} ions which can be explained by the crystallization of the Er-silicate with RTA process.

Controlling the growth of the B-type $Er_2Si_2O_7$ phase at the nanometer scale can be promising for the development of Er-based optical materials. Lo Savio *et al.* have shown that triclinic phase is the most promising candidate for efficient luminescence in IR range [28,35]. However, exact nature of the phase which provides the more intense emission is still matter of debates since some authors

claim that the monoclinic phase provide most efficient luminescence [29].

4. Conclusion

Correlative analyses of the optical, structural and chemical properties at the nanoscale allowed us to identify the luminescence properties of nanostructures erbium disilicate phases in silica elaborated by magnetron sputtering. First, the results show an important effect of annealing strategy on the phase separation between SiO_2 and $Er_2Si_2O_7$ phases, and on the crystallization of the latter. We highligthed the formation of an original honeycomb Er-silicates compound presenting an amorphous nature using a classical annealing at 1000°C and triclinic $Er_2Si_2O_7$ for RTA at 1200°C. Besides, the enhancement of luminescence in the IR range resulting from the crystallization of the erbium disilicate phase has been clearly demonstrated.

CRediT authorship contribution statement

Etienne Talbot: Conceptualization, Methodology, Validation, Formal analysis, Visualization, Investigation, Writing – review & editing. Fabrice Gourbilleau: Conceptualization, Methodology, Validation, Formal analysis, Visualization, Investigation, Writing – review & editing, Funding acquisition. Rémi Demoulin and Sonia Guehairia: Investigation, Validation, Visualization, Formal analysis, Writing – original draft Hocine Merabet: Project administration, Funding acquisition, Writing – review & editing Philippe Pareige: Supervision, Writing – review & editing Julien Cardin and Christophe Labbé: Investigation, Validation, Writing – review & editing Marzia Carrada: Investigation, Validation, Writing – review & editing.

Data availability

Data will be made available on request.

Declaration of Competing Interest

The authors declare that they have no known competing financial interests or personal relationships that could have appeared to influence the work reported in this paper.

Acknowledgements

Appendix A. Supporting information

Supplementary data associated with this article can be found in the online version at doi:10.1016/j.jallcom.2022.166947.

References

[1] N. Daldosso, L. Pavesi, Low-Dimensional Silicon as a Photonic Material, Elsevier, Amsterdam, 2008, pp. 314–334, https://doi.org/10.1016/B978-008044528-1.50010-5

[2] A. Kenyon, Recent developments in rare-earth doped materials for optoelectronics, Prog. Quantum Electron. 26 (4–5) (2002) 225–284, https://doi.org/10.1016/S0079-6727(02)00014-9

[3] J. Li, O. Zalloum, T. Roschuk, C. Heng, J. Wojcik, P. Mascher, Light emission from rare-earth doped silicon nanostructures, Adv. Opt. Technol. 2008 (2008) 295601, https://doi.org/10.1155/2008/295601

[4] S. Cueff, C. Labbé, J. Cardin, J.-L. Doualan, L. Khomenkova, K. Hijazi, O. Jambois, B. Garrido, R. Rizk, Efficient energy transfer from Si-nanoclusters to Er ions in silica induced by substrate heating during deposition, J. Appl. Phys. 108 (6) (2010) 64302, https://doi.org/10.1063/1.3481375

[5] A.J. Kenyon, Erbium in silicon, Semicond. Sci. Technol. 20 (12) (2005) R65–R84, https://doi.org/10.1088/0268-1242/20/12/r02

[6] D. Das, A. Samanta, Quantum size effects on the optical properties of nc-Si QDs embedded in an a-SiOx matrix synthesized by spontaneous plasma processing, Phys. Chem. Chem. Phys. 17 (7) (2015) 5063–5071, https://doi.org/10.1039/C4CP05126B

[7] A. Polman, Erbium implanted thin film photonic materials, J. Appl. Phys. 82 (September 1996) (1997) 1–39, https://doi.org/10.1063/1.366265

[8] G. Franzo, S. Boninelli, D. Pacifici, F. Priolo, F. Iacona, C. Bongiorno, Sensitizing properties of amorphous Si clusters on the 1.54-μ m luminescence of Er in Si-rich SiO_2, Appl. Phys. Lett. 82 (22) (2003) 3871, https://doi.org/10.1063/1.1579555

[9] P. Kik, A. Polman, Exciton-erbium energy transfer in si nanocrystal-doped sio2, Mater. Sci. Eng.: B 81 (1) (2001) 3–8, https://doi.org/10.1016/S0921-5107(00)00667-X

[10] P.G. Kik, M.L. Brongersma, a. Polman, Strong exciton-erbium coupling in Si nanocrystal-doped SiO_2, Appl. Phys. Lett. 76 (17) (2000) 2325, https://doi.org/10.1063/1.126334

[11] M. Fujii, M. Yoshida, Y. Kanzawa, S. Hayashi, K. Yamamoto, 1.54 μ m photoluminescence of $Er^{3.}$ doped into SiO_2 films containing Si nanocrystals: Evidence for energy transfer from Si nanocrystals to $Er^{3.}$ Appl. Phys. Lett. 71 (9) (1997) 1198–1200, https://doi.org/10.1063/1.119624

[12] G. Franzò, V. Vinciguerra, F. Priolo, The excitation mechanism of rare-earth ions in silicon nanocrystals, Appl. Phys. A 69 (1) (1999) 3–12, https://doi.org/10.1007/s003390050967

[13] A. Lesage, D. Timmerman, D.M. Lebrun, Y. Fujiwara, T. Gregorkiewicz, Hot-carrier-mediated impact excitation of $Er^{3.}$ ions in SiO_2 sensitized by Si Nanocrystals, Appl. Phys. Lett. 113 (3) (2018) 031109, https://doi.org/10.1063/1.5042013

[14] L. Khomenkova, F. Gourbilleau, J. Cardin, R. Rizk, Towards an enhanced coupling between the er ions and si nanoclusters, Phys. E: Low. -Dimens. Syst. Nanostruct. 41 (6) (2009) 1048–1051, https://doi.org/10.1016/j.physe.2008.08.016

[15] A. Thogersen, J. Mayandi, T. Finstad, A. Olsen, S. Diplas, M. Mitome, Y. Bando, The formation of Er-oxide nanoclusters in SiO_2 thin films with excess Si, J. Appl. Phys. 106 (1) (2009) 14305, https://doi.org/10.1063/1.3148266

[16] G. Beainy, C. Frilay, P. Pareige, F. Gourbilleau, E. Talbot, On the interplay between Si-Er-O segregation and erbium silicate ($Er_2 Si_2 O_7$) formation in Er-doped SiO_X thin films, J. Alloy. Compd. 755 (2018) 55–60, https://doi.org/10.1016/j.jallcom.2018.04.310

[17] E. Talbot, R. Lardé, P. Pareige, L. Khomenkova, K. Hijazi, F. Gourbilleau, Nanoscale evidence of erbium clustering in Er-doped silicon-rich silica, Nanoscale Res. Lett. 8 (1) (2013) 1–8, https://doi.org/10.1186/1556-276X-8-39

[18] Y. Gao, Q. Fu, H. Shen, D. Li, D. Yang, Correlation of efficient luminescence with crystal structures of y-$Er_2 Si_2 O_7$ and α -$Er_2 Si_2 O_7$ in Er-doped silicon oxide films, J. Mater. Sci. 54 (19) (2019) 12668–12675, https://doi.org/10.1007/s10853-019-03783-3

[19] J. Li, Q. Lin, Z. Sun, Photoluminescence of er silicates on microstructured si substrate, J. Lumin. 132 (2) (2012) 325–329, https://doi.org/10.1016/j.jlumin.2011.08.040 ⟨https://www.sciencedirect.com/science/article/pii/S002223131100487X⟩.

[20] H. Xu, Z. Chen, Y. Zhao, J. Guo, W. Liu, X. Wang, M. Huo, Y. Sui, The upconversion luminescence from visible to near-infrared in pyrosilicate c-$er_2 si_2 o_7$, J. Alloy. Compd. 897 (2022) 162963, https://doi.org/10.1016/j.jallcom.2021.162963

[21] N. Prtljaga, D. Navarro-Urrios, A. Tengattini, A. Anopchenko, J.M. Ramírez, J.M. Rebled, S. Estradé, J.-P. Colonna, J.-M. Fedeli, B. Garrido, L. Pavesi, Limit to the erbium ions emission in silicon-rich oxide films by erbium ion clustering, Opt. Mater. Express 2 (9) (2012) 1278–1285, https://doi.org/10.1364/OME.2.001278

[22] J. Zheng, W. Ding, C. Xue, Y. Zuo, B. Cheng, J. Yu, Q. Wang, G. Wang, H. Guo, Highly efficient photoluminescence of er2sio5 films grown by reactive magnetron sputtering method, J. Lumin. 130 (3) (2010) 411–414, https://doi.org/10.1016/j.jlumin.2009.10.005

[23] Y. Gao, H. Shen, D. Li, D. Yang, Efficient sensitized photoluminescence of er silicate in silicon oxide films embedded with amorphous silicon clusters, part i: fabrication, Opt. Mater. Express 9 (11) (2019) 4329–4338, https://doi.org/10.1364/OME.9.004329

[24] W. Lefebvre-Ulrikson, F. Vurpillot, X. Sauvage (Eds.), p. ix, Academic Press, 2016, https://doi.org/10.1016/B978-0-12-804647-0.01002-0

[25] S. Cueff, C. Labbé, B. Dierre, J. Cardin, L. Khomenkova, F. Fabbri, T. Sekiguchi, R. Rizk, Cathodoluminescence and photoluminescence comparative study of erbium-doped silicon-rich silicon oxide, J. Nanophotonics 5 (1) (2011) 1–17, https://doi.org/10.1117/1.3549701

[26] R.L. Savio, M. Miritello, F. Iacona, A.M. Piro, M.G. Grimaldi, F. Priolo, Thermal evolution of Er silicate thin films grown by rf magnetron sputtering, J. Phys.: Condens. Matter 20 (45) (2008) 454218, https://doi.org/10.1088/0953-8984/20/45/454218

[27] M. Miritello, R. LoSavio, F. Iacona, G. Franzò, A. Irrera, A.M. Piro, C. Bongiorno, F. Priolo, Efficient luminescence and energy transfer in erbium silicate thin films, Adv. Mater. 19 (12) (2007) 1582–1588, https://doi.org/10.1002/adma.200601692

[28] R. LoSavio, M. Miritello, A.M. Piro, F. Priolo, F. Iacona, The influence of stoichiometry on the structural stability and on the optical emission of erbium silicate thin films, Appl. Phys. Lett. 93 (2) (2008) 21919, https://doi.org/10.1063/1.2957034

[29] Y. Gao, H. Shen, J. Cao, D. Li, D. Yang, Control of the formation and luminescent properties of polymorphic erbium silicates on silicon, Opt. Mater. Express 9 (4)

(2019) 1716–1727, https://doi.org/10.1364/OME.9.001716 ⟨http://opg.optica.org/ome/abstract.cfm?URI=ome-9-4-1716⟩.

[30] M.W. Sckerl, S. Guldberg-Kjaer, M. RysholtPoulsen, P. Shi, J. Chevallier, Precipitate coarsening and self organization in erbium-doped silica, Phys. Rev. B 59 (21) (1999) 13494–13497, https://doi.org/10.1103/PhysRevB.59.13494

[31] M. Thuvander, H.-O. Andrén, K. Stiller, Q.-H. Hu, A statistical method to detect ordering and phase separation by APFIM, Ultramicroscopy 73 (1) (1998) 279–285, https://doi.org/10.1016/S0304-3991(97)00168-X

[32] J. Felsche, Polymorphism and crystal data of the rare-earth disilicates of type r.e.$_2$ si$_2$ o$_7$, J. Less Common Met. 21 (1) (1970) 1–14, https://doi.org/10.1016/0022-5088(70)90159-1

[33] A. Maqsood, Phase transformations in er$_2$ si$_2$ o$_7$ ceramics, J. Mater. Sci. Lett. 16 (1997) 837–840, https://doi.org/10.1023/A:1018542828045

[34] L. Kepinski, L. Krajczyk, W. Mista, Interaction of ce1 − x er$_x$ o$_{2-y}$ nanoparticles with sio$_2$ -effect of temperature and atmosphere, J. Solid State Chem. 209 (2014) 42–55, https://doi.org/10.1016/j.jssc.2013.10.025

[35] X.J. Wang, T. Nakajima, H. Isshiki, T. Kimura, Fabrication and characterization of er silicates on sio$_2$ /si substrates, Appl. Phys. Lett. 95 (4) (2009) 041906, https://doi.org/10.1063/1.3192407

[36] P. Pellegrino, B. Garrido, J. Arbiol, C. Garcia, Y. Lebour, J.R. Morante, Site of Er ions in silica layers codoped with Si nanoclusters and Er, Appl. Phys. Lett. 88 (12) (2006) 121915, https://doi.org/10.1063/1.2190267